# Spatial Resolution of Microwave Tomography for Detection of Myocardial Ischemia and Infarction–Experimental Study on Two-Dimensional Models

Serguei Y. Semenov, Robert H. Svenson, Alexander E. Bulyshev, Alexander E. Souvorov, Alexei G. Nazarov, Yuri E. Sizov, Vitaly G. Posukh, Andrey V. Pavlovsky, Pavel N. Repin, and George P. Tatsis

***Abstract*—In this paper, the experimental study of spatial resolution of microwave tomography was performed. Our microwave tomographic system with operational frequencies of 0.9 and 2.36 GHz and with signal-to-noise ratio of 30 dB allowed us to achieve a spatial resolution between 7.3–9.5 mm and 6.3–7.8 mm at the former and latter frequencies, respectively. It was shown in experiments, with structurally complicated objects, that the spatial resolution of about the same distances can be expected in a practical application of microwave tomography to detect areas of myocardial ischemia and infarction.**

***Index Terms*—Microwave tomography, myocardial infarction, spatial resolution.**

## I. Introduction

MICROWAVE tomography is a new imaging modality that may have a number of important applications in medicine. In previous papers [1]–[4], we have described the development of two-dimensional (2-D) and three-dimensional (3-D) systems and reconstruction algorithms. We have demonstrated the imaging possibilities using these algorithms and devices for imaging phantoms and biological objects of different dielectric contrasts. However, we have not systematically studied the spatial resolution that can be achieved experimentally.

Theoretically, in the far field, the spatial resolution of tomographic imaging systems is a function of the wavelength $(\lambda)$ of radiation in the medium. Therefore, microwave tomography can not compete with X-ray tomography in terms of the spatial resolution. However, microwave tomography has a number of advantages, including the possibility of imaging physiological changes, which have been discussed elsewhere [1], [5]. Devaney [6] suggested that the limit of resolution in diffraction tomography was roughly about $\lambda/\sqrt{2}$. Bolomey and Pichot [7] estimated that spatial resolution was limited to about one-half of the wavelength in the medium in which the test object is immersed. However, for near-field imaging, Meaney *et al.* [8] have estimated that image reconstruction "is fundamentally unlimited by wavelength" and "is restricted by signal-to-noise" ratio. Chen and Chew [9] have experimentally observed in near fields a "resolution which is better than quarter-wavelength" for a high contrast, but not dispersive and lossy objects. They suggested that the major reason for such "super resolution" at a small fraction of wavelength was the utilization of a nonlinear reconstruction algorithm.

From a practical point-of-view, a number of issues need to be taken into account in the spatial resolution of microwave tomography of full-scale high dielectric contrast objects such as the human body. These issues are: 1) wavelength of the radiation; 2) image reconstruction algorithm; 3) properties of the microwave tomographic system such as signal-to-noise ratio; 4) acquisition time and system stability (in the case of physiologically active and dynamic objects); 5) geometry of the tomographic working chamber (vertical and radial dimensions); and 6) the number of emitters and receivers and properties of the biological object (tissue) to be imaged (attenuation, dielectric contrast, inhomogeneity, anisotropy, etc). Therefore, the study of the experimentally achievable spatial resolution of microwave tomography, which will cover the whole variety of imaginable cases, is almost impossible.

Our overall goal is to detect myocardial ischemia and infarction with the help of microwave tomography. Utilizing dielectric spectroscopy, we have studied the changes of myocardial dielectric properties (canine and pig studies) caused by acute ischemia and chronic infarction [10], [11]. The measured dielectric properties of normal *in situ* canine myocardium and their changes during acute ischemia and chronic infarction are briefly summarized in Section IV-B. Therefore, it is particularly important to study the applicability of microwave tomography to spatially resolve ischemic or infarcted areas of the myocardium (with contrast of about 10%). Consideration will also be given in Section IV-B to the choice of the experimental models for myocardial ischemia and infarction.

The study was performed at frequencies of 0.9 and 2.36 GHz. The experimental setup and images reconstruction method are described in Sections II and III, respectively. Section IV covers

Manuscript received November 25, 1998. This work was supported by the Carolinas HealthCare System Foundation through the Carolinas Medical Center and the Carolinas Heart Institute under a grant.

S. Y. Semenov, R. H. Svenson, A. E. Bulyshev, A. E. Souvorov, and G. P. Tatsis are with the Laser and Applied Technologies Laboratory, Carolinas Heart Institute, Carolinas Medical Center, Charlotte, NC 28203 USA (e-mail: ssemenov@carolinas.org).

A. G. Nazarov, Y. E. Sizov, A. V. Pavlovsky, and P. N. Repin are with the Biophysical Research Laboratory, Kurchatov Institute of Atomic Energy, Moscow, Russia.

V. G. Posukh is with the Institute of Laser Physics, Novosibirsk, Russia.

Publisher Item Identifier S 0018-9480(00)02770-8.

the description of the experimental phantoms and models. The experimental results are presented and discussed in Section V.

## II. Experimental Setup and Methods

Experiments were conducted using a prototype of the 3-D microwave tomographic system switched to its 2-D mode. A detailed system description has been presented elsewhere [4]. The basic operation frequency of the system was 2.36 GHz. To meet the purpose of this study, the system was modified to operate at an additional frequency of 0.9 GHz. The transmitter power was 1 W. The polarization of the vector $\mathbf{E}$ of the emitted electromagnetic (EM) radiation was linear in the vertical direction. The vertical component of the scattered EM field $\mathbf{E}_s$ was measured. The current prototype allows measurement of attenuation in the tomographic working chamber up to 120 dB with a signal-to-noise ratio of about 30 dB.

The object under study was located on a rotating support plate on the axis of the cylindrical tomographic working chamber with a height of 40 cm and a diameter of 60 cm. A detailed description of the measurement procedure has been presented elsewhere [4]. An automatic motion system and motion-control system place the receiving antenna at various points on the circle with radius 11 cm behind a 2-D object. The transmitter was located at a 17.9-cm distance from the center of the tomographic chamber.

The microwave tomographic chamber was filled with deionized water (2.36 GHz, $\varepsilon = 78.0 - j10.2$) or salt solution (0.9 GHz, $\varepsilon = 79.0 - j21.5$). A coaxial probe and an HP8753D Network Analyzer were used to measure dielectric properties of materials and solutions. In addition, online temperature control of the solution in the working chamber was used during experiments.

## III. Image-Reconstruction Method

We have previously presented a method for image reconstruction based on the generalization of the Newton procedure [3]. This nonlinear reconstruction procedure allows us to obtain images with medium and high dielectric contrast in 2-D geometry. We also demonstrated the qualitative reconstruction of a 2-D mathematical model of the human torso [3].

In the current study, we utilized the reconstruction procedure presented in [3]. The reconstruction of both experimental and simulated data have been performed in 2-D geometry. The direct problem was solved in a fine mesh of 512 nodes over angle and of 200 nodes over radius in polar coordinate system. The inverse problem was solved in a Cartesian mesh of 46 × 46 nodes. All calculations were performed on a DEC ALPHA-8200 server.

## IV. Experimental Models

### A. Two-Point Phantoms

We started the experimental part with the classical experiments of spatial resolution. A two-point phantom, which consisted of two small objects, was placed into the center of the microwave tomographic chamber. The distance between the objects was varied (from 2 to 15 mm) to find out at what distance we could distinguish one object from another.

Three different phantoms were used in the two-point experiments. At 2.36 GHz, the first phantom **(P1)** was a rectangular object ($\varepsilon_p = 70.0(\pm 5.0) - \mathbf{j}9.0(\pm 0.7)$) with two cylindrical holes with a diameter of 6.5 mm filled with immersion liquid. The second phantom **(P2)** consisted of two metallic rods with a diameter of 4 mm. The reason for having these two phantoms, evaluated at 2.36 GHz, was to model two quite different cases in terms of the values of the scattered EM field. The first phantom (P1) models a low contrast case (near 10%), closer to the situation of ischemic/infarcted areas located inside of normal myocardium. In this case, the amplitude of the scattered EM field was relatively small. The second phantom (P2) had high dielectric contrast and high amplitude of the scattered EM field. At 0.9 GHz, the phantom **(P3)** consisted of two plastic tubes with a diameter of 11 mm filled with sand.

At 2.36 GHz for P1 and P2, we filled the tomographic working chamber with deionized water ($\varepsilon_{\text{wat}} = 78.0 - \mathbf{j}10.2$). To be consistent with both total attenuation inside of the tomographic chamber and the value of the scattered EM field, at a frequency of 0.9 GHz for P3, we filled the tomographic working chamber with a salt solution ($\varepsilon_{\text{sal}} = 79.0 - j21.5$). This does not change the wavelength, but significantly increases the attenuation coefficient. The phantoms were irradiated from 64 directions. The receiving antenna was moved around the phantom on the circle with radius 11 cm. It measured the scattered EM field at 32 points.

*Definition of the Resolution Function:* To estimate the spatial resolution, the reconstructed images of the two-point object were analyzed in the following way. In each image, we made a cross section through the centers of the two objects. As a result, we observed such a function, presented in the upper right-hand-side portion of Fig. 1(a). As a resolution function, we used the ratio ***(Umin/Umax)*** between minimum and maximum (mean of two maximums) of the above curve. We have defined that objects can be tomographically resolved if ratio ***Umin/Umax*** is less than 0.5–0.8, i.e., between half of the height criteria and Rayleigh criteria.

### B. "Ischemic-Infarcted" Zone

We have shown [10], [11] that at a frequency of 2.4 GHz, 2-h acute myocardial ischemia causes a 5% decrease in both parts of the complex myocardial dielectric permittivity. On the other hand, chronic myocardial infarction (from two weeks to five months) causes an increase (about 8%–10%) in both parts of the complex myocardial dielectric permittivity. The degree of the observed changes was more pronounced at lower frequencies. For example, at a frequency of 1 GHz, two-week chronic myocardial infarction caused an increase in $\varepsilon''$ up to 15% and at a frequency of 0.2 GHz, about 20%.

In this study, the possibility of microwave tomography for detecting ischemic or infarcted areas of the myocardium with dimensions of about 6–8 mm and a dielectric contrast of about 5%–10% was tested in the following way. We created a 2-D experimental phantom of the heart (Fig. 2) with dielectric properties $\varepsilon_p = 70.0(\pm 5.0) - \mathbf{j}9.0(\pm 0.7)$ at 2.36 GHz. The phantom

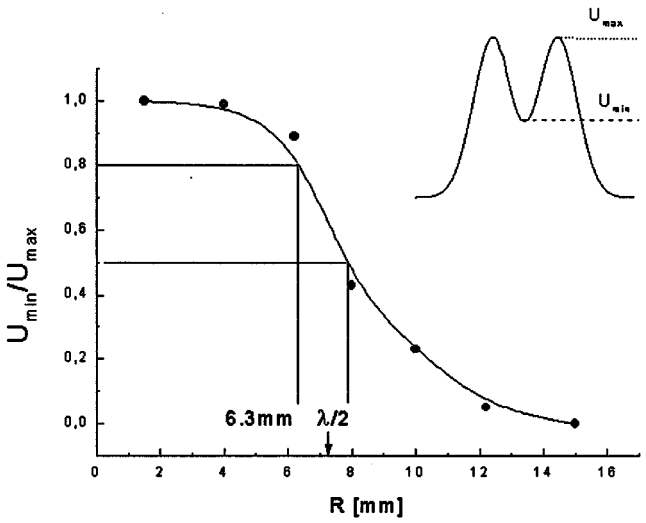


(a)

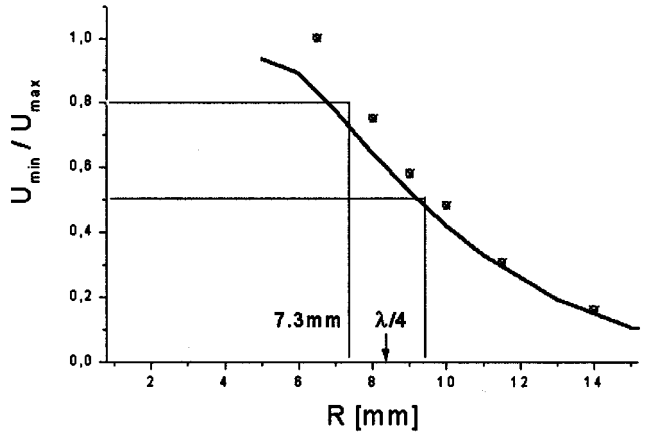


(b)

Fig. 1. Resolution ratio ***Umin/Umax*** as a function of distance between cylindrical objects. (a) At 2.36 GHz. (b) At 0.9 GHz.

was placed in the center of the tomographic chamber filled with deionized water $\varepsilon_w = 78.0 - \mathbf{j}10.2$. Three inhomogeneities were inserted into the wall of the phantom. They simulate the following three different cases:

1) acute ischemic zone with $\varepsilon_{\text{ischemic}} = 60.0(\pm 5.0) - \mathbf{j}7.3(\pm 0.7)$;
2) chronic infarcted zone with $\varepsilon_{\text{infarct}} = 78.0 - \mathbf{j}10.2$;
3) composite model containing infarcted and ischemic tissues.

The last case is of particular interest in cardiac arrhythmia detection. The ischemic (boundary) area of the myocardium located around (or inside) of the chronic infarcted (or scar) tissue is a major source of cardiac arrhythmogenicity.

### C. Objects with Complicated Structure

To extend our study for imaging of objects with a complicated structure, we constructed additional phantoms.

At 2.36 GHz, the phantom ***(cp1)*** was a "Tree of Life," which is the logo of the Carolinas Medical Center (Fig. 3) The distance between details was about 5–6 mm. The phantom with dielectrical properties $\varepsilon_p = 70.0(\pm 5.0) - \mathbf{j}9.0(\pm 0.7)$ was placed in the center of the tomographic working chamber filled with deionized water $(\varepsilon_w = 78.0 - \mathbf{j}10.2)$.

At a frequency of 0.9 GHz, we used a phantom ***(cp2)***, presented in Fig. 4. This phantom had different distances between details, ranging from 8 to 20 mm. The phantom with dielectrical properties $\varepsilon_p = 70.0(\pm 5.0) - \mathbf{j}18.0(\pm 0.7)$ was placed in the center of the tomographic working chamber filled with a salt solution $(\varepsilon_{\text{sal}} = 77.5 - \mathbf{j}20.0)$.

## V. Results and Discussion

### A. Spatial Resolution Study on Two-Point Phantoms

The results of the rectangular phantom (P1) reconstruction at 2.36 GHz are presented in Fig. 5(A). The distances $(D)$ between the cylindrical holes are 4 and 8 mm. The results of the P2 phantom (two metallic rods) reconstruction at the same frequency are presented in Fig. 5(B) for the distances of 6 and 8 mm between objects. In the case of 8-mm distance, the reconstructed images reveal two clearly separated holes in the first case (P1) and two clearly separated objects in the second case (P2). When the distance was 4 mm between two holes (P1), the images were qualitatively reconstructed. Similarly, when the distance was 6 mm between two objects (P2), the images were qualitatively reconstructed. However, at these distances, the reconstructed holes (objects) are not clearly separated. Comparing reconstruction examples of the two kinds of phantoms, it is possible to conclude that, despite different amplitudes of the scattered EM fields, the results of the reconstruction of phantom structures are similar. For the rectangular phantom (P1, low-contrast case), we reasonably reconstructed the values of the dielectrical properties.

With the resolution criteria defined above, a spatial resolution between 6.3–7.8 mm was achieved experimentally at 2.36 GHz. It should be emphasized that the wavelength of radiation in water at 2.36 GHz is 1.44 cm. Therefore, we achieved a spatial resolution that is about or slightly better than half of the wavelength. It is interesting that under the digital criteria, we concluded that the distance of about 4–6 mm is below the spatial resolution (Fig. 1). However, having simple visual criteria, we can distinguish one object from another even in this case (Fig. 5). It has to be emphasized that the images presented in Fig. 5(A) and (B) and the spatial resolution results presented in Fig. 1(a) were achieved without any image preprocessing (filtering, countering, etc.).

The experiments and an analysis of the results at 0.9 GHz were conducted exactly the same way. We tried to conduct experiments at both frequencies under conditions as similar as possible in terms of total attenuation, signal-to-noise ratio, and the amplitude of the scattered EM field. This allowed us to compare the spatial resolution at both frequencies. The resolution ratio ***Umin/Umax*** as a function of the distance between two objects (plastic tubes) is presented in Fig. 1(b). With the resolution criteria defined above, we found that, at a frequency of 0.9 GHz, the spatial resolution was between 7.3–9.5 mm. This is slightly worse compared with a frequency of 2.36 GHz. However, compared to the wavelength in salt solution ($\lambda/4 = 8.3$ mm), the experimentally achieved spatial resolution at 0.9 GHz was about or even better than a quarter of the wavelength.

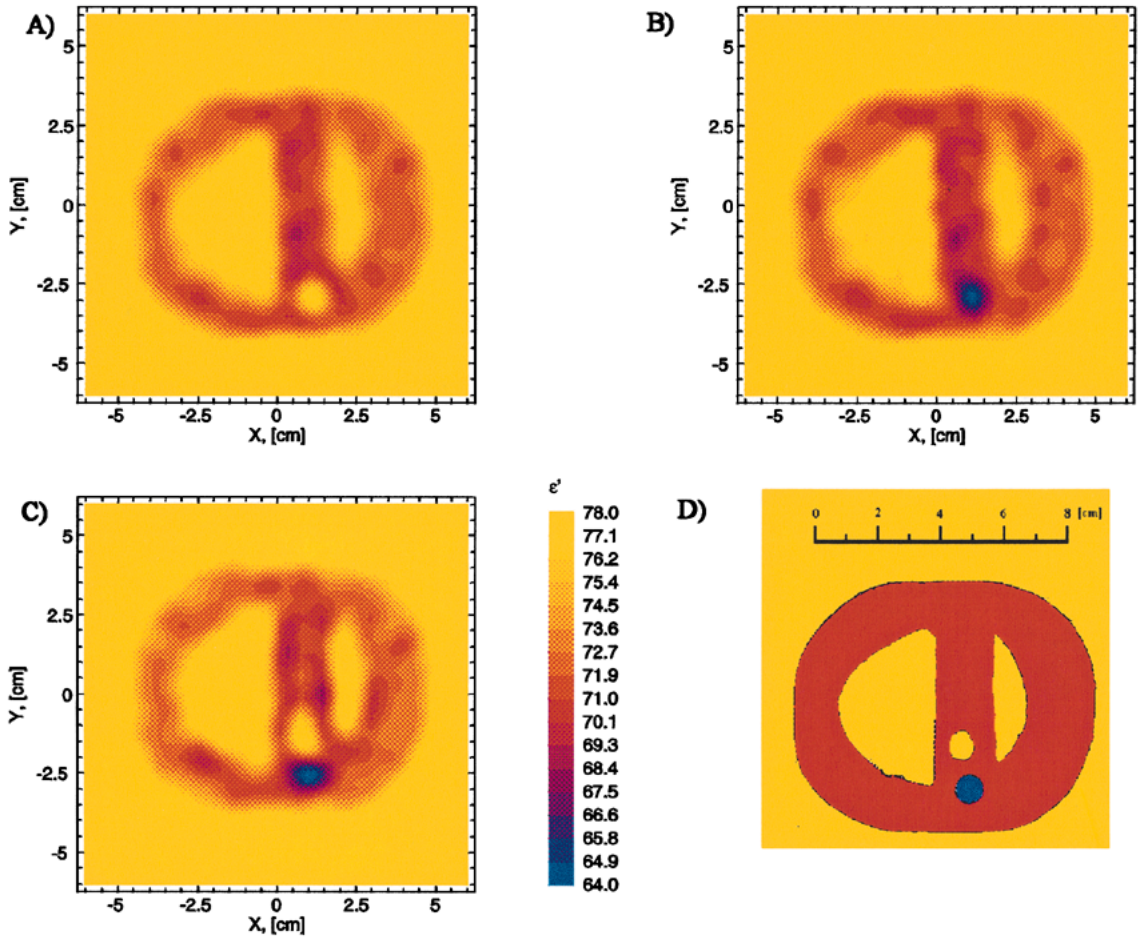


Fig. 2. Reconstructed images of the 2-D model of the heart with three inhomogeneities. (A) Model of the chronic infarction. (B) Model of acute ischemia. (C) Composite model of infarcted-ischemic area. (D) View of experimental phantom.

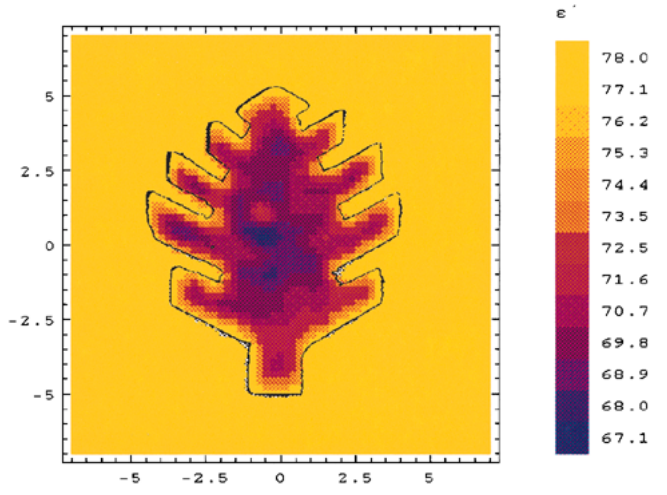


Fig. 3. Reconstructed image of the complex object ("Tree of Life" logo of the Carolinas Medical Center) at 2.36 GHz. Black contour around the image is the boundary of the phantom.

We compared the experimental results with a mathematical simulation. To simulate the experiment, we calculated the interaction of a 2-D TM wave with two cylinders with $\varepsilon_{\mathrm{cyl}} = 4.0 - j0.0$. We estimated that the noise figure in our experiments was about 3%. We added 2.5% random noise to simulated scattered EM field. The theoretical resolution function is added to Fig. 1(b). The theoretical resolution function fits the experimental data reasonably well. Therefore, it is possible to conclude that our understanding of the EM-field distribution inside of the tomographic chamber and the measurements of the EM fields are correct. Another conclusion, using this experimental setup and reconstruction algorithm, is that improvement of the signal-to-noise ratio is the only one way to improve spatial resolution.

As conclusion from this experimental part, the spatial resolution between 6.3–7.8 mm at 2.36 GHz and between 7.3–9.5 mm at 0.9 GHz was experimentally achieved. Comparing with the wavelength in medium, the achieved spatial resolution is about or slightly better than half of the wavelength at first frequency (2.36 GHz) and about or better than a quarter of the wavelength at a 0.9 GHz.

### *B. Detection of Ischemic and Infarcted Zones*

The images presented in Fig. 2 reveal all inhomogeneities. Both ischemic and infarcted areas can be detected. More importantly, they can be distinguished from each other. Therefore, the complexity of an object (in scale of presented study) should not result in deterioration of the spatial resolution achieved in the two-point cases.

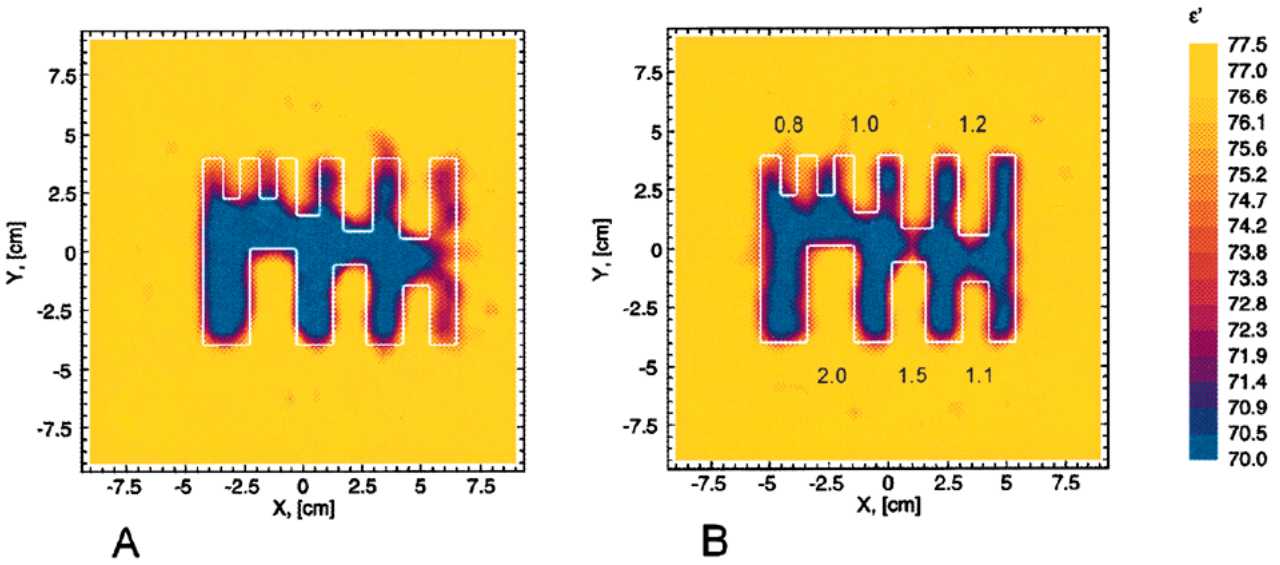


Fig. 4. Reconstructed image of the complex object at 0.9 GHz for: (A) experimental phantom and (B) simulated phantom with 3% random noise. White contour is a phantom boundary.

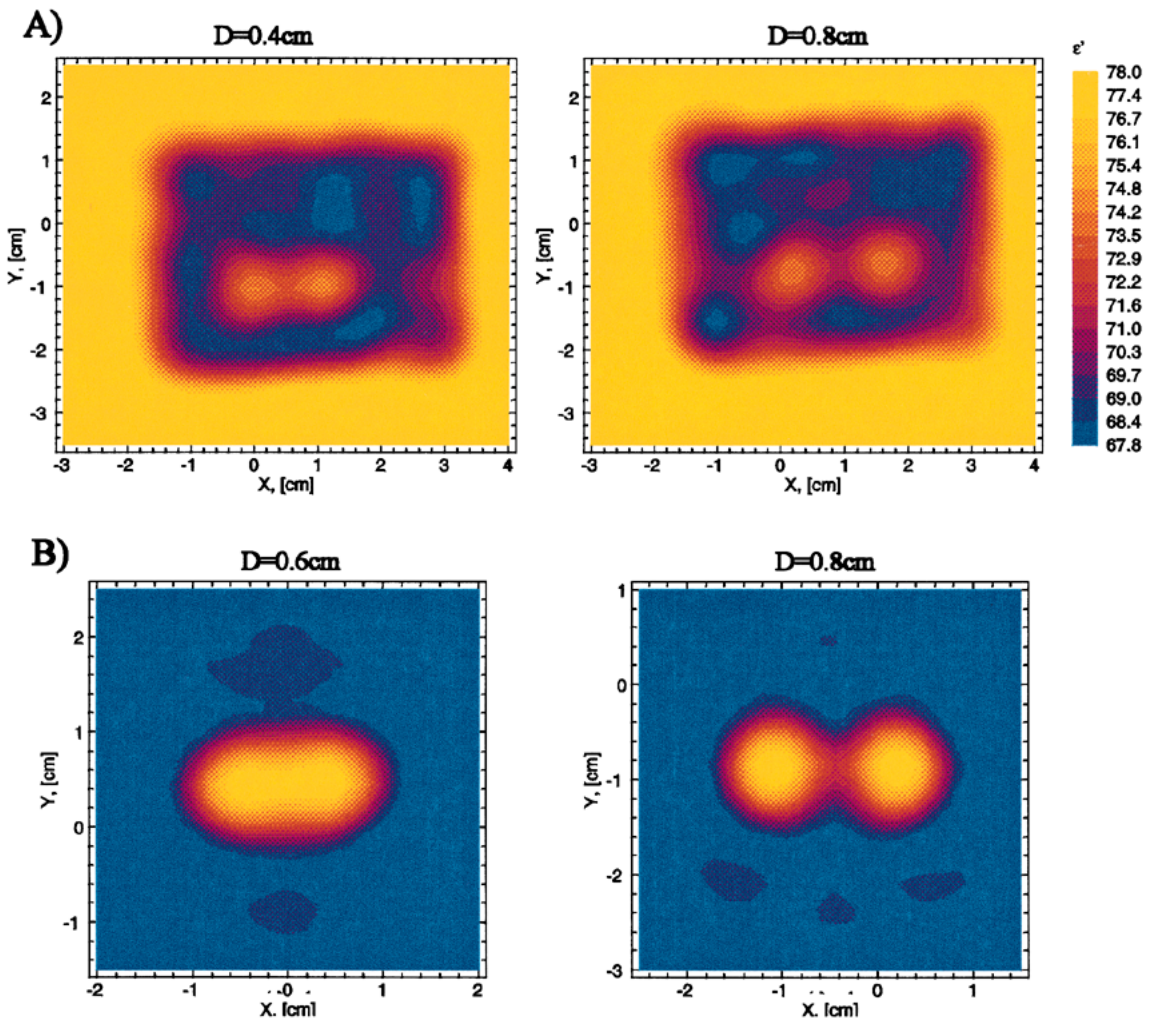


Fig. 5. Images reconstruction at 2.36 GHz for different distances ($\mathbf{D}$) between cylindrical holes (objects) for $\varepsilon'$. (A) For rectangular phantom. (B) For two-metallic rods.

### C. Imaging of Objects with a Complicated Structure

The experimental phantom ***(cp1)*** and reconstructed image are presented in Fig. 3 for 2.36 GHz. The reconstructed image reveals the structure of the phantom. Visually, all details are separated. We also created a phantom with the same structure having a distance between details of about 3 mm. In this case, only a qualitative image was achieved. All details were washed away. Concluding this part, having the current tomographic system with signal-to-noise ratio about 30 dB and the current reconstruction algorithm, we have demonstrated that spatial resolution of about 6.5 mm at 2.36 GHz can be achieved despite a structurally complex object.

The reconstructed images of the complex phantom ***(cp2)*** are presented in Fig. 4 for 0.9 GHz for such cases (A—experimental phantom, B—simulated model with 3% random noise). Both simulated and experimental images are closer to each other. This proves an estimation of the noise level in our experimental system, which was estimated as about 3% at 0.9 GHz. As can be seen from both images, the spatial resolution at 0.9 GHz is lying between 8.0–10.0 mm. This is the same range as was achieved earlier in two-point experiments, despite a structurally complex object.

The generalization of these experimental results to the case of a full-scale object such as a human torso is not so simple. In an ideal situation, a spatial resolution of about 6–8 mm can be expected. However, in reality, there will be a certain number of factors, which could worsen spatial resolution. These include physiological activity of living objects (including respiratory and cardiac cycle), technical problems (signal-to-noise ratio, number of emitters and receivers, etc.), and mathematical reconstruction problems (3-D geometry with vector EM field, number of calculation grids, etc.). Earlier [3, Fig. 8], we have demonstrated successful reconstruction of the 2-D mathematical model of the torso with small inhomogeneities, incorporated into a myocardial wall of the heart. It can be expected that the large scale of an object will not cause a deterioration in spatial resolution compared with the experimental studies on smaller scale objects.

## VI. Conclusion

The microwave tomographic system with operational frequencies of 0.9 and 2.36 GHz and with a signal-to-noise ratio of 30 dB allowed us to achieve a spatial resolution between 7.3–9.5 mm and 6.3–7.8 mm at two frequencies, respectively. At 2.36 GHz, the spatial resolution is about or slightly better than half of the wavelength (7.2 mm) in medium. At 0.9 GHz, the spatial resolution is about or better than quarter of the wavelength (8.3 mm) in the medium. The spatial resolution of about the same distances can be expected in a practical application of the microwave tomography to detect areas of the myocardial ischemia and infarction.

## References

[1] S. Y. Semenov, R. H. Svenson, A. E. Bulyshev, A. E. Souvorov, V. Y. Borisov, Y. E. Sizov, A. N. Starostin, K. Dezern, G. P. Tatsis, and V. Y. Baranov, "Microwave tomography: Two-dimensional system for biological imaging," *IEEE Trans. Biomed. Eng.*, vol. 43, pp. 869–877, Sept. 1996.

[2] S. Y. Semenov, A. E. Bulyshev, A. E. Souvorov, R. H. Svenson, Y. E. Sizov, V. Y. Borisov, V. G. Posukh, I. M. Kozlov, A. G. Nazarov, and G. P. Tatsis, "Microwave tomography: Theoretical and experimental investigation of the iteration reconstruction algorithm," *IEEE Trans. Microwave Theory Tech.*, vol. 46, pp. 133–141, Feb. 1998.

[3] A. E. Souvorov, A. E. Bulyshev, S. Y. Semenov, R. H. Svenson, A. G. Nazarov, Y. E. Sizov, and G. P. Tatsis, "Microwave tomography: A two-dimensional newton iterative scheme," *IEEE Trans. Microwave Theory Tech.*, vol. 46, pp. 1654–1659, Nov. 1998.

[4] S. Y. Semenov, R. H. Svenson, A. E. Boulyshev, A. E. Souvorov, A. G. Nazarov, Y. E. Sizov, A. Pavlovsky, V. Y. Borisov, B. G. Voinov, G. Simonova, A. N. Starostin, G. P. Tatsis, and V. Y. Baranov, "Three dimensional microwave tomography. Experimental prototype of the system and vector born reconstruction method," *IEEE Trans. Biomed. Eng.*, vol. 46, pp. 937–946, Aug. 1999.

[5] L. E. Larsen and J. H. Jacobi, Eds., *Medical Application of Microwave Imaging*. New York: IEEE Press, 1986.

[6] A. J. Devaney, "Current research topics in diffraction tomography," in *Inverse Problems in Scattering and Imaging*, M. Bertero and E. K. Pike, Eds. New York: Adam Hilger, 1992, pp. 47–58.

[7] J. C. Bolomey and C. Pichot, "Some applications of diffraction tomography to electromagnetics—The particular case of microwaves," in *Inverse Problems in Scattering and Imaging*, M. Bertero and E. K. Pike, Eds. New York: Adam Hilger, 1992, pp. 319–344.

[8] P. M. Meaney, K. D. Paulsen, A. Hartov, and R. C. Crane, "Microwave imaging for tissue assessment: Initial evaluation in multitarget tissue-equivalent phantoms," *IEEE Trans. Biomed. Eng.*, vol. 43, pp. 878–890, Sept. 1996.

[9] F. C. Chen and W. C. Chew, "Experimental verification of super resolution in nonlinear inverse scattering," *Appl. Phys. Lett.*, vol. 72, no. 23, pp. 3080–3082, 1998.

[10] S. Y. Semenov, R. H. Svenson, K. R. Dezern, M. E. Quinn, M. Thompson, and G. P. Tatsis, "Myocardial ischemia and infarction can be detected by microwave spectroscopy. 1. Experimental evidence," in *Proc. IEEE 18th Eng. Medicine and Biol. Annu. Int. Conf.*, Amsterdam, The Netherlands, Oct. 31–Nov. 3 1996, pp. 5.4.1–5.

[11] S. Semenov, R. Svenson, G. Simonova, A. Bulyshev, A. Souvorov, Y. Sizov, A. Nazarov, V. Borisov, A. Pavlovsky, M. Taran, and G. Tatsis, "Dielectric properties of canine acute and chronic myocardial infarction at a cell relaxation spectrum. 1. Experiment," in *Proc. IEEE 19th Eng. Medicine and Biol. Annu. Int. Conf.*, Chicago, IL, Oct. 30 –Nov. 2 1997, pp. 1.0.1–PB11.

[12] A. Devaney, "A computer simulation study of diffraction tomography," *IEEE Trans. Biomed. Eng.*, vol. BME-30, pp. 377–386, July 1983.

**Serguei Y. Semenov** was born in Moscow, Russia, in 1959. He received the M.S. degree in physics from the Moscow State Lomonosov University, Moscow, Russia, in 1982 , and the Ph.D. in biophysics and radiobiology from the Moscow Biophysical Institute, Moscow, Russia, in 1985.

Since 1988, he has been with the Kurchatov Institute of Atomic Energy, Moscow, Russia. He is currently the Director of Biophysical Laboratory at this institution and a Research Scientist at the Carolinas Medical Center, Charlotte, NC. His research interests are EM radiation interaction with biological tissues and nonionizing radiation tomography.

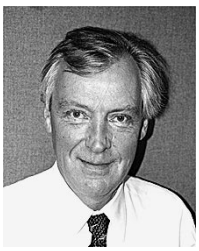

**Robert H. Svenson** received the B.A. degree from Lawrence University, Appleton, WI, in 1963, and the M.D. degree from the University of Chicago School of Medicine, Chicago, IL, in 1969.

In 1972, he completed his residency in Internal Medicine at University of Chicago Hospitals and Clinics. He was a Post-Doctoral Fellow in the Division of Cardiology, Duke University Medical Center, Durham, NC. Since 1975, he has been a Cardiologist and Electrophysiologist for Sanger Clinic, Charlotte, NC. In addition, he has served as the Medical Director of the Laser and Applied Technologies Laboratory, Carolinas Medical Center, Charlotte, NC. His research interests are cardial physiology and electrophysiology.

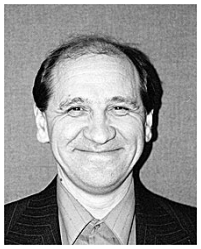

**Alexander E. Bulyshev** was born in Novosibirsk, Russia, in 1953. He received the M.S. degree in physics from the Novosibirsk State University, Novosibirsk, Russia, in 1975, the Ph.D. degree in physics from the Latvian University, Riga, Latvia, in 1979, and the Professor of Physics degree from Tomsk University, Tomsk, Russia, in 1994.

From 1975 to 1996, he was a Researcher at the Institute of Theoretical and Applied Mechanics, Novosibirsk, Russia. He is currently a Research Scientist in the Laser and Applied Technologies Laboratory, Carolinas Medical Center, Charlotte, NC. His research interests are inverse problems and transfer of radiation.

**Alexander E. Souvorov** was born in Novosibirsk, Russia, in 1953. He received the M.S. degree in physics from the Novosibirsk State University, Novosibirsk, Russia, in 1975, and the Ph.D. degree in physics from the Latvian University, Riga, Latvia, in 1979.

From 1975 to 1986, he was a Researcher at the Institute of Theoretical and Applied Mechanics, Novosibirsk, Russia. From 1986 to 1996, he was a Researcher at the Institute of Heat and Mass Transfer, Minsk, Belarussia. He is currently a Research Scientist at the Laser and Applied Technologies Laboratory, Carolinas Medical Center, Charlotte, NC. His research interests are theoretical and calculational physics.

**Alexei G. Nazarov** received the M.S. degree in radio physics and the Ph.D. degree in antennas and microwave technologies from the Moscow Power Engineering Institute (Technical University), Moscow, Russia, in 1992 and 1997, respectively.

He is currently with the Biophysics Research Laboratory, Kurchatov Institute of Atomic Energy, Moscow, Russia. His major research interest is system design and microwave equipment.

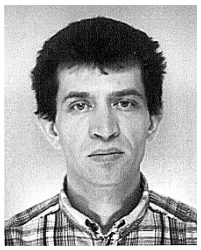

**Yuri E. Sizov** was born in Troitsk, Moscow Region, Russia, in 1961. He received the M.S. degree in the electronic engineering from the Moscow Electronic Institute, Moscow, Russia, in 1984.

He is currently an Electronic Engineer in the Biophysical Research Laboratory, Kurchatov Institute of Atomic Energy, Moscow, Russia. He is expert in electronic and computer engineering.

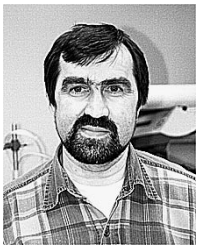

**Vitaly G. Posukh** received the M.S. degree in physics and applied mathematics from the Novosibirsk State University, Novosibirsk, Russia, in 1975.

From 1976 to 1991, he was a Research Scientist at the Institute of Theoretical and Applied Mechanics, Siberian Branch of the Russian Academy of Sciences, Novosibirsk, Russia. He is currently a Principal Engineering Specialist at the Institute of Laser Physics, Siberian Branch of the Russian Academy of Sciences, Novosibirsk, Russia.

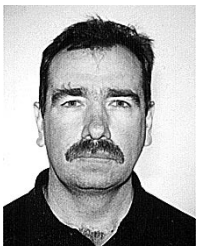

**Andrey V. Pavlovsky** received the M.S. degree in computer technologies from the Moscow Power Engineering Institute, Moscow, Russia.

He is currently an Electronic Engineer in the Laboratory of Applied Biophysics, Kurchatov Institute of Atomic Energy, Moscow, Russia.

**Pavel N. Repin** received the M.S. degree in physics from the Moscow Electronic Technologies Institute, Moscow, Russia, in 1975.

From 1987 to 1997 , he was a Microwave Engineer in the Scientific Research Institute of Microdevices, Moscow, Russia. He is currently a Microwave Engineer in the Laboratory of Applied Biophysics, Kurchatov Institute of Atomic Energy, Moscow, Russia.

**George P. Tatsis** received the B.S. degree in biology from the University of North Carolina, Chapel Hill, in 1981, and the M.S. degree in biology from the University of North Carolina, Charlotte, in 1989.

From 1982 to 1988, he conducted cardiovascular research at the Heineman Medical Research Laboratories. Since 1988, he has served as the Administrative Director of the Laser and Applied Technologies Laboratory, Carolinas Medical Center, Charlotte, NC. In 1993, he was also appointed Director of Clinical Research of the Carolinas Heart Institute.